Letter

Magnetotransport in topological materials and nonlinear Hall effect via first-principles electronic interactions and band topology

Dhruv C. Desai [1], Lauren A. Tan [1], Jin-Jian Zhou [2], Shiyu Peng [1], Jinsoo Park [1,3] and Marco Bernardi [1,*]

[1] *Department of Applied Physics and Materials Science and Department of Physics, California Institute of Technology, Pasadena, California 91125, USA*

[2] *School of Physics, Beijing Institute of Technology, Beijing 100081, China*

[3] *Department of Physics, Pohang University of Science and Technology, Pohang 37673, Korea*

(Received 10 October 2025; accepted 24 February 2026; published 23 March 2026)

Topological effects arising from the Berry curvature lead to intriguing transport signatures in quantum materials. Two such phenomena are the chiral anomaly and nonlinear Hall effect (NLHE). A unified description of these transport regimes requires a quantitative treatment of both band topology and electron scattering. Here, we show accurate predictions of the magnetoresistance in topological semimetals and NLHE in noncentrosymmetric materials by solving the Boltzmann transport equation with electron-phonon (*e*-ph) scattering and Berry curvature computed from first principles. We apply our method to study magnetotransport in a prototypical Weyl semimetal, TaAs, and the NLHE in strained monolayer WSe_2, bilayer WTe_2, and bulk $BaMnSb_2$. In TaAs, we find a chiral contribution to the magnetoconductance that is positive and increases with magnetic field, consistent with experiments. We show that *e*-ph interactions can significantly modify the Berry curvature dipole and its dependence on temperature and Fermi level, highlighting the interplay of band topology and electronic interactions in nonlinear transport. The computed nonlinear Hall response in $BaMnSb_2$ is in agreement with experiments. By adding the Berry curvature to first-principles transport calculations, our work advances the quantitative analysis of a wide range of linear and nonlinear transport phenomena in quantum materials.

DOI: 10.1103/fl5l-dhn3

Band topology is a central theme in quantum materials and is responsible for emergent behaviors such as robust edge states [1–3], topological superconductivity [4], spin Hall effects [5,6], and unconventional transport regimes [7–9]. This physics is relevant for wide-ranging applications in electronics, spintronics, and quantum technologies [10,11]. The theory of Berry curvature and topological invariants has provided a deeper understanding of topological phases [3]. Recent advances have led to the prediction and discovery of topological transport regimes, including the chiral anomaly in topological semimetals [12–14], the nonlinear Hall effect (NLHE) in noncentrosymmetric materials [15–17], and novel nonlinear transport regimes in magnetic systems [18–20].

Although predictions of chiral anomaly in solids have a long history [21], this effect has been observed only recently in topological Weyl semimetals in the form of a large negative longitudinal magnetoresistance (LMR) [22–29]. The negative LMR is caused by charge pumping between two Weyl cones when parallel electric and magnetic fields are applied, and experiments on Weyl semimetals have achieved a decrease in resistivity by more than 50% at large magnetic fields [22,24]. This behavior contrasts with conventional magnetotransport in metals, where the LMR is positive and increases with magnetic field. The NLHE is a more recent development in topological transport [30] and has become an exciting research topic, with measurements reported in a wide range of materials [31–39]. Unlike the chiral anomaly, the nonlinear Hall response does not require a magnetic field or magnetization, but rather is an intrinsic higher-order response to an electric field [15].

Previous theoretical work combined the Boltzmann transport equation (BTE) with Berry curvature from model Hamiltonians and heuristic treatments of electronic scattering to study the chiral anomaly [40,41] and NLHE [16]. These studies have advanced qualitative understanding of topological transport while focusing on models with simplifying approximations such as constant relaxation times and Berry curvature dipole (BCD) from tight binding.

First-principles calculations using density functional theory [42] and Wannier functions [43] have enabled quantitative studies of electronic band topology and Berry curvature [44,45]. In parallel, first-principles calculations of electron-phonon (*e*-ph) interactions and phonon-limited electronic transport [46–53] have seen rapid progress, including in topological materials [54,55]. However, studies combining these two advances are almost absent, with the exception of recent calculations by Lihm and Park [56] predicting an enhancement of NLHE in GeTe due to *e*-ph interactions. First-principles calculations of the chiral anomaly have not been reported, and a method to study topological magnetotransport and the NLHE in a unified framework is still missing.

In this Letter, we show calculations that combine the BTE with first-principles *e*-ph interactions and Berry curvature. Using this method, we study magnetotransport in a prototypical Weyl semimetal, TaAs, and compute the nonlinear

*Contact author: bmarco@caltech.edu

 ©2026 American Physical Society

Hall response and *e*-ph interaction-renormalized BCDs in three materials: bilayer WTe_2 (BL-WTe_2), strained monolayer WSe_2 (ML-WSe_2), and bulk $BaMnSb_2$. Our approach allows us to access both classical (Lorentz) and quantum (chiral) contributions to magnetotransport by importance sampling of Brillouin zone regions with large Berry curvature. Our calculations in TaAs predict transport properties in very good agreement with experiments and shed light on the relative magnitudes of classical and chiral contributions as a function of Fermi level. Our nonlinear transport results reveal a strong interplay between the *e*-ph interactions and BCD, and predict temperature trends of the NLHE consistent with experiments. The approach described in this work paves the way for quantitative studies of intrinsic (*e*-ph limited) magnetotransport and nonlinear transport properties in quantum materials, advancing the microscopic understanding of transport regimes governed by band topology.

We describe the chiral anomaly starting from the semiclassical equations of motion (EOM). In a material with applied electric and magnetic fields (**E** and **B**, respectively), the coupled EOM for the position (**r**) and momentum (**k**) of an electron wave packet are modified by the Berry curvature $\Omega_{n\mathbf{k}}$ [see Eq. (3.8) in [57], Eq. (5.8) in [58], and Ref. [59]]. Keeping terms up to $O(\Omega_{n\mathbf{k}})$ in the Berry curvature, and neglecting the orbital magnetization contribution, to be explored in future work, the EOM can be written as [see Eq. (6) in Ref. [40] and derivations in the Supplemental Material (SM) [60]]:

$$\dot{\mathbf{r}} = \frac{1}{1+\frac{e}{\hbar}\mathbf{B}\cdot\mathbf{\Omega}_{n\mathbf{k}}}\Big[\mathbf{v}_{n\mathbf{k}} + \frac{e}{\hbar}\mathbf{E}\times\mathbf{\Omega}_{n\mathbf{k}} + \frac{e}{\hbar}(\mathbf{v}_{n\mathbf{k}}\cdot\mathbf{\Omega}_{n\mathbf{k}})\mathbf{B}\Big],$$
$$\dot{\mathbf{k}} = \frac{(-e/\hbar)}{1+\frac{e}{\hbar}\mathbf{B}\cdot\mathbf{\Omega}_{n\mathbf{k}}}\Big[\mathbf{E} + \mathbf{v}_{n\mathbf{k}}\times\mathbf{B} + \frac{e}{\hbar}(\mathbf{E}\cdot\mathbf{B})\mathbf{\Omega}_{n\mathbf{k}}\Big], \quad (1)$$

where e is the electron charge, $\hbar$ is Planck's constant, and $\mathbf{v}_{n\mathbf{k}}$ is the band velocity for a Bloch state with crystal momentum $\mathbf{k}$ and band index n. Using these EOMs, we derive a steady-state linearized BTE that takes into account the Berry curvature contribution (see SM for derivations [60, 61]):

$$\frac{1}{1+\frac{e}{\hbar}\mathbf{B}\cdot\mathbf{\Omega}_{n\mathbf{k}}}\Big[\mathbf{v}_{n\mathbf{k}} + \frac{e}{\hbar}(\mathbf{v}_{n\mathbf{k}}\cdot\mathbf{\Omega}_{n\mathbf{k}})\mathbf{B} + \frac{e}{\hbar}(\mathbf{v}_{n\mathbf{k}}\times\mathbf{B})\nabla_{\mathbf{k}}\mathbf{F}_{n\mathbf{k}}\Big]$$
$$= \frac{1}{\mathcal{N}_{\mathbf{q}}}\sum_{m,\nu\mathbf{q}}\Big(1+\frac{e}{\hbar}\mathbf{B}\cdot\mathbf{\Omega}_{m\mathbf{k}+\mathbf{q}}\Big)W^{\nu\mathbf{q}}_{n\mathbf{k},m\mathbf{k}+\mathbf{q}}(\mathbf{F}_{n\mathbf{k}} - \mathbf{F}_{m\mathbf{k}+\mathbf{q}}), \quad (2)$$

where $\mathbf{F}_{n\mathbf{k}}$ measures the change in electronic occupations relative to equilibrium, $f_{n\mathbf{k}} - f^0_{n\mathbf{k}} = (\partial f^0_{n\mathbf{k}}/\partial\varepsilon_{n\mathbf{k}})\, e\mathbf{E}\cdot\mathbf{F}_{n\mathbf{k}}$, and $f^0_{n\mathbf{k}}$ is the Fermi-Dirac distribution [62]. The right-hand side of Eq. (2) is the *e*-ph collision term, where $W^{\nu\mathbf{q}}_{n\mathbf{k},m\mathbf{k}+\mathbf{q}}$ is the scattering rate from state $|n\mathbf{k}\rangle$ to $|m\mathbf{k}+\mathbf{q}\rangle$ due to absorption or emission of a phonon (with wave vector $\mathbf{q}$ and mode index ν) as defined in [62], and $\mathcal{N}_{\mathbf{q}}$ is the number of $\mathbf{q}$ points in the summation. The factor $(1+\frac{e}{\hbar}\mathbf{B}\cdot\mathbf{\Omega}_{m\mathbf{k}+\mathbf{q}})$ in Eq. (2) can be viewed as a Berry-phase correction to the electronic density of states [63].

After solving Eq. (2) for $\mathbf{F}_{n\mathbf{k}}$, we compute the conductivity tensor [62]

$$\sigma_{ab} = \frac{e^2 S}{\mathcal{N}_{\mathbf{k}} V k_B T}\sum_{n\mathbf{k}}\Big(1+\frac{e}{\hbar}\mathbf{B}\cdot\mathbf{\Omega}_{n\mathbf{k}}\Big)f^0_{n\mathbf{k}}\big(1-f^0_{n\mathbf{k}}\big)\dot{\mathbf{r}}_a\mathbf{F}_{n\mathbf{k}}(\mathbf{B})_b, \quad (3)$$

where a and b are Cartesian directions while S, V, and $\mathcal{N}_{\mathbf{k}}$ are the spin degeneracy, unit-cell volume, and number of $\mathbf{k}$ points, respectively. Note that the term in $\dot{\mathbf{r}}$ proportional to $\mathbf{E}$ contributes to transport only at second order in $\mathbf{E}$, and is not included in calculations of conductivity and chiral anomaly, which are responses linear in $\mathbf{E}$. The implicit dependence of σ on the Berry curvature gives rise to chiral transport in Weyl semimetals. In particular, the anomalous velocity term in Eq. (1) causes the conductivity to increase with magnetic field (negative LMR), in contrast with the usual decrease caused by the Lorentz force in simple metals [12].

The NLHE can be described within the same theoretical framework. We expand the expression for the current density $\mathbf{J}$ to second order in the applied electric field [15]:

$$J_a = \sigma_{ab}E_b + \chi_{abc}E_bE_c, \quad (4)$$

where we sum over repeated indices; σ_{ab} is defined above and its transverse (Hall) components are zero in systems with time-reversal symmetry [17]. Therefore, the leading-order Hall response is given by the second-order term $\chi_{abc}E_bE_c$. To obtain an expression for the third-rank conductivity tensor χ, we start from the current

$$\mathbf{J} = \frac{-Se}{\mathcal{N}_{\mathbf{k}}V}\sum_{n\mathbf{k}} f_{n\mathbf{k}}\dot{\mathbf{r}}. \quad (5)$$

Setting $\mathbf{B}$=0 in Eq. (3) and using the above expression for $\mathbf{J}$, we obtain (see SM [60])

$$\chi_{abc} = \epsilon_{abd}T_{dc} + \epsilon_{acd}T_{db}, \quad (6)$$

where ϵ_{abc} is the Levi-Civita tensor and we define

$$T_{ab} = \frac{e^3 S}{2\mathcal{N}_{\mathbf{k}}V\hbar k_B T}\sum_{n\mathbf{k}} f^0_{n\mathbf{k}}\big(1-f^0_{n\mathbf{k}}\big)(\mathbf{\Omega}_{n\mathbf{k}})_a(\mathbf{F}_{n\mathbf{k}})_b. \quad (7)$$

This formula reduces the computation of the rank-three tensor χ_{abc} to the computation of the rank-two tensor T_{ab}. Previous work on NLHE used a constant relaxation time approximation [16], in which case this tensor becomes $T_{ab} = \frac{e^3 S\tau}{2\hbar^2}D_{ab}$, where D_{ab} is the BCD defined in band theory without interactions [16]:

$$D_{ab} = \int\frac{d^d\mathbf{k}}{(2\pi)^d}\Omega_{n\mathbf{k},a}\frac{\partial f^{(0)}_{n\mathbf{k}}}{\partial k_b}. \quad (8)$$

Here, we modify this expression to take into account *e*-ph scattering, and define an *e*-ph renormalized BCD:

$$D^{e\text{-ph}}_{ab} = \frac{2\hbar^2}{e^3 S\langle\tau\rangle}T_{ab}$$
$$= \frac{\hbar}{\mathcal{N}_{\mathbf{k}}Vk_BT\langle\tau\rangle}\sum_{n\mathbf{k}} f^0_{n\mathbf{k}}\big(1-f^0_{n\mathbf{k}}\big)(\mathbf{\Omega}_{n\mathbf{k}})_a(\mathbf{F}_{n\mathbf{k}})_b, \quad (9)$$

where $\langle\tau\rangle$ is the average relaxation time obtained from the state-dependent relaxation times using $\langle\tau\rangle^{-1} =$

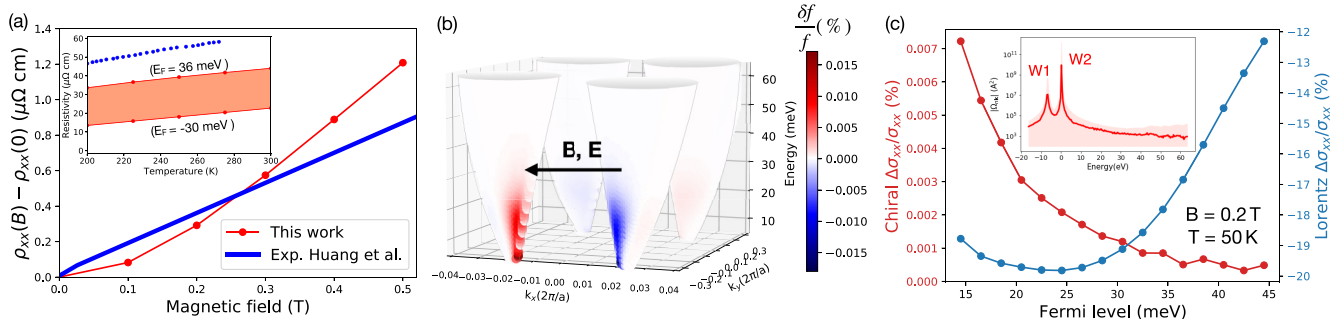

FIG. 1. Magnetotransport in TaAs. (a) Longitudinal magnetoresistance, $\rho_{xx}(\mathbf{B})-\rho_{xx}(0)$, vs magnetic field, computed at 100 K for $E_F =$ 35 meV and compared with experiments from Ref. [23]. The inset shows the resistivity vs temperature for Fermi levels between roughly ±35 meV of the Weyl nodes. (b) Weyl cones in TaAs, color-coded according to the change in electronic occupations from the chiral term under parallel electric and magnetic fields, computed at 50 K for $B = 0.2$ T. Note that the white points in the red region are a plotting artifact. (c) Chiral and Lorentz contributions to magnetoconductance vs Fermi level relative to the Weyl node, using the same settings as in (b). The inset shows the Berry curvature as a function of energy for TaAs, with the Weyl cones labeled as W1 and W2.

$\sum_{n\mathbf{k}}(\partial f_{n\mathbf{k}}/\partial\varepsilon_{n\mathbf{k}})\tau^{-1}_{n\mathbf{k}} / \sum_{n\mathbf{k}}(\partial f_{n\mathbf{k}}/\partial\varepsilon_{n\mathbf{k}})$. As we show in the following, the e-ph renormalization, which is encoded in the BTE solution $\mathbf{F}_{n\mathbf{k}}$, has a significant effect on the BCD and is essential to make accurate predictions of nonlinear Hall response.

To study these transport phenomena, we implement these equations in the open source code PERTURBO [62]. For each material, the electronic ground state, band structure, and lattice dynamics are calculated using QUANTUM ESPRESSO [64,65]. We then use PERTURBO to compute and interpolate the e-ph interactions on dense momentum grids and obtain converged transport properties [62]; the interpolation uses Wannier functions obtained from WANNIER90 [66]. We compute the Berry curvature in PERTURBO by implementing the formalism developed by Wang *et al.* [see Eq. (27) in Ref. [44]]. To compute the conductivity in Eq. (3), we develop an adaptive **k**-point sampling technique that can optimally sample states with a large Berry curvature. Additional details are provided in the SM [60].

We first discuss magnetotransport and chiral anomaly in TaAs. Figure 1(a) shows the classical (Lorentz) contribution to the LMR, $\rho_{xx}(\mathbf{B}) - \rho_{xx}(0)$, as a function of magnetic field for a Fermi level $E_F = 35$ meV above the Weyl node at 100 K temperature. The Lorentz contribution is defined as the conductance obtained by solving the BTE in Eq. (2) for $\mathbf{\Omega}_{n\mathbf{k}}=0$, and thus without the chiral term [second term in brackets in Eq. (2)]. Our computed LMR is in very good agreement with experimental data on TaAs from Ref. [23]. The inset shows the phonon-limited resistivity at zero magnetic field as a function of temperature for E_F values between roughly ±35 meV of the Weyl node, which agrees well with calculations of zero field resistivity in Refs. [55,67]. For temperatures above ∼200 K, where transport is usually limited by e-ph interactions, our predicted resistivity is within 30% of measured values [23]. These results point to a dominant role for the e-ph interactions in controlling the resistivity and magnetotransport in TaAs.

In our calculations, TaAs shows 12 pairs of Weyl nodes, with 8 pairs at zero energy (W2) and 4 pairs at −10 meV energy (W1), consistent with previous calculations [23,68] and angle-resolved photoemission spectroscopy data [69]. Figure 1(b) shows two pairs of W2 Weyl cones in TaAs, with colors indicating the computed change in electronic occupations at steady state induced by the magnetic field, $[f(\mathbf{B},\mathbf{E})\text{-}f(0,\mathbf{E})]/f(0,\mathbf{E})$, under parallel electric and magnetic fields. This effect is caused by the chiral contribution in the BTE—the second term in brackets in Eq. (2): since the sign of the Berry curvature is opposite for the two Weyl cones, the chiral term in the BTE causes an increase in occupations for one cone and a decrease for the other cone in the pair. This creates a net charge pumping effect between Weyl cones, causing the conductivity to increase with magnetic field in our calculations, consistent with previous predictions [40,41].

To quantify the increase in conductivity, we compute the chiral contribution to the longitudinal magnetoconductance, defined as the conductance obtained by solving the BTE without the Lorentz term [third term in Eq. (2)], shown in Fig. 1(c) (red curve) as a function of Fermi level at 50 K for $B = 0.2$ T. The chiral contribution is large for Fermi levels near the Weyl cones and decays sharply as E_F increases. Since the chiral anomaly is proportional to the Berry curvature, this decay can be attributed to the rapid decrease of the Berry curvature away from the W2 Weyl cones [inset of Fig. 1(c)]. Note that the divergence of the Berry curvature near the W2 nodes leads to a breakdown of the semiclassical approximation, which restricts our calculations of chiral and classical contributions to $E_F \gtrsim 10$ meV from the Weyl nodes (see SM for discussion [60]).

The classical (Lorentz) term dominates in this energy window due to the rapid decrease of the chiral contribution. This trend is clearly seen by computing the Lorentz contribution to the longitudinal magnetoconductance [blue curve in Fig. 1(c)], which is found to be orders of magnitude greater than the chiral contribution in the semiclassical regime (here, $E_F > 15$ meV from the Weyl nodes). We conclude that the Lorentz term dominates magnetotransport in TaAs in the semiclassical regime. Experimental results from Ref. [25] suggest that the chiral contribution may become dominant when the Fermi level is close to the Weyl nodes. Transport calculations in that energy window—within a few meV of the Weyl nodes—will require a quantum treatment of transport beyond the BTE and will be explored in future work.

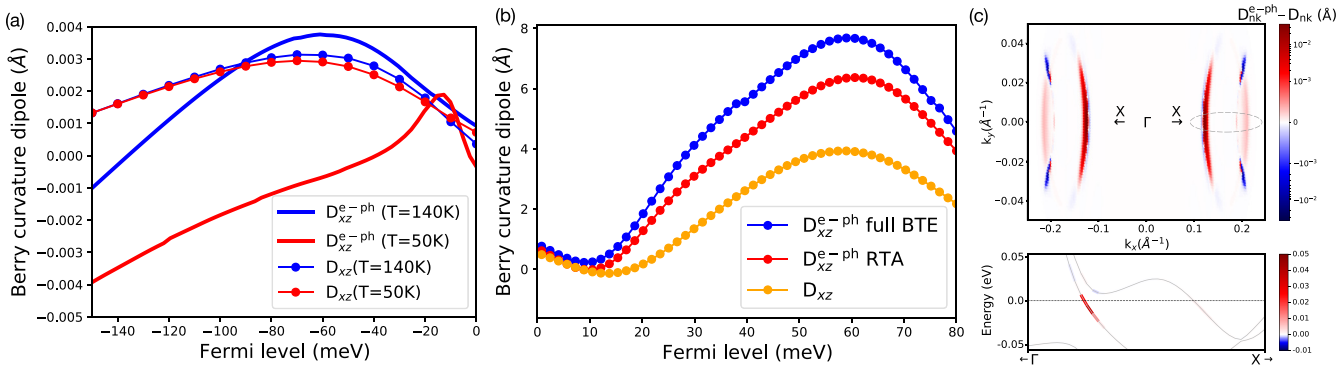

FIG. 2. (a) Berry curvature dipole D_{xz}, computed using the Berry curvature alone using Eq. (8), compared with the e-ph renormalized BCD, $D_{xz}^{e\text{-ph}}$, in strained ML-WSe_2. The results are shown at two temperatures, 50 (red) and 140 K (blue), as a function of Fermi level in the valence band. (b) Different approximations for the BCD in BL-WTe_2, computed at 100 K without e-ph interactions (orange), and with e-ph renormalization using the RTA (red) or the full BTE solution (blue). (c) e-ph induced BCD enhancement, shown by plotting the difference of BCD integrands, $D_{n\mathbf{k}}^{e\text{-ph}} - D_{n\mathbf{k}}$, in $\mathbf{k}$ space in BL-WTe_2 (upper panel) and the same quantity mapped onto the band structure for the region in the dashed oval (lower panel).

Next, we discuss calculations of the NLHE, focusing first on two-dimensional materials, strained ML-WSe_2 and BL-WTe_2, where previous work has reported the presence of a BCD [31,70]. In ML-WSe_2, it has been shown that breaking the C_3 symmetry by applying a uniaxial strain along the a axis induces a finite BCD and Hall response [39,70]. Therefore, we conduct our calculations on ML-WSe_2 with 3% strain along the a axis.

Addressing the temperature dependence of the BCD and nonlinear Hall response is an important feature of our approach. Figure 2(a) shows the BCD in strained ML-WSe_2 computed at two temperatures (50 and 140 K) for different values of the Fermi level in the valence band. For each calculation, we compare the usual BCD, D_{xz} defined in Eq. (8) and computed using the Berry curvature alone, with the e-ph renormalized BCD, $D_{xz}^{e\text{-ph}}$ defined in Eq. (9), where e-ph scattering is taken into account using the solution of the BTE ($\mathbf{F}_{n\mathbf{k}}$). We find that the e-ph interactions modify the BCD significantly and change its dependence on temperature and Fermi level [Fig. 2(a)]. The commonly studied BCD computed directly from the Berry curvature (D_{xz}) is nearly constant between 50 and 140 K. In contrast, the e-ph interactions introduce a pronounced temperature dependence, and the renormalized BCD increases significantly from 50 to 140 K, consistent with measurements by Qin *et al.* [39].

In BL-WTe_2, the e-ph interactions enhance the BCD but do not qualitatively change the temperature or Fermi-level dependence [Fig. 2(b)]. Figure 2(b) additionally compares the e-ph renormalized BCD ($D_{xz}^{e\text{-ph}}$) in BL-WTe_2 computed using two different approximations: the "full" solution of the BTE [$\mathbf{F}_{n\mathbf{k}}$ obtained by solving Eq. (2)], which is more accurate and is used throughout this Letter, and the simpler relaxation time approximation (RTA), where the form $\mathbf{F}_{n\mathbf{k}} = \tau_{n\mathbf{k}}\mathbf{v}_{n\mathbf{k}}$ is assumed for the deviation of the occupations from equilibrium (note that this version of the RTA still uses first-principles state- and temperature-dependent relaxation times $\tau_{n\mathbf{k}}$, and thus is far more accurate than the "textbook" RTA with an empirical constant relaxation time). The renormalized BCD obtained by solving the BTE is 2 times greater than the BCD value without e-ph renormalization. The RTA can capture this trend, but it predicts a more modest (50%) enhancement relative to the band theory BCD, with the advantage of bypassing the BTE solution and thus saving significant computational effort.

To study the origin of this enhancement, we analyze the contributions to the renormalized BCD by rewriting Eq. (9) as

$$D^{e\text{-ph}} \equiv \sum_{n\mathbf{k}} D_{n\mathbf{k}}^{e\text{-ph}}. \tag{10}$$

In Fig. 2(c), we analyze the effects of e-ph interactions by plotting the difference of the e-ph renormalized and band-theory BCD integrands in $\mathbf{k}$ space, $D_{n\mathbf{k}}^{e\text{-ph}} - D_{n\mathbf{k}}$, in BL-$WTe_2$. We find that the BCD enhancement is concentrated in small regions of the Brillouin zone and arises from electronic states on or near the Weyl cones in correspondence of small electron energy gaps, which enhance the Berry curvature.

Using the RTA, $\mathbf{F}_{n\mathbf{k}} = \mathbf{v}_{n\mathbf{k}}\tau_{n\mathbf{k}}$, where $\tau_{n\mathbf{k}}$ is the e-ph relaxation time, and thus the renormalized BCD can be written as the band-theory BCD integrand $D_{n\mathbf{k}}$ modified in $\mathbf{k}$ space by the ratio of the state-dependent relaxation time to its average value:

$$D_{zx,n\mathbf{k}}^{e\text{-ph}} \approx D_{zx,n\mathbf{k}} \frac{\tau_{n\mathbf{k}}}{\langle\tau\rangle}. \tag{11}$$

In BL-WTe_2, we have verified that the factor $\tau_{n\mathbf{k}}/\langle\tau\rangle$ is greater than 1 for electronic states with large BCD values, which explains the overall increase in BCD. A similar enhancement is also observed for the BCD obtained from the full BTE solution. The substantial changes in BCD induced by e-ph interactions highlight the need for an accurate description of both e-ph scattering and band topology for quantitative modeling of nonlinear Hall transport.

Finally, we study the NLHE in $BaMnSb_2$, a bulk Dirac material with a small gap at the Dirac nodes, where a strong nonlinear Hall response near room temperature has been shown in recent experiments [36]. The computed e-ph renormalized BCD, shown in Fig. 3(a), exhibits a pronounced dependence on temperature and Fermi level. At low temperature, the BCD shows a sharp characteristic peak for $E_F =$ 30 meV relative to the conduction band edge, consistent with

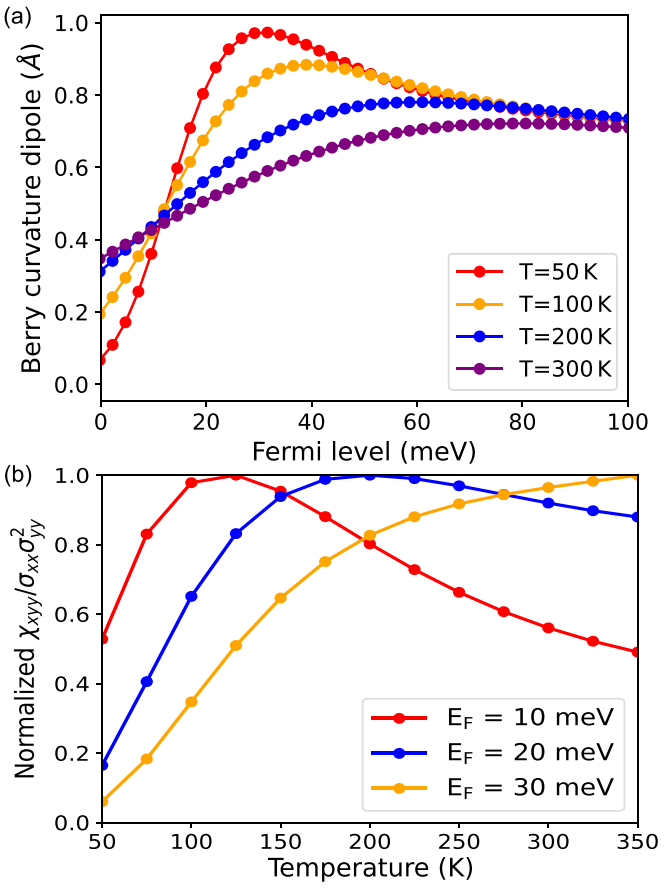

FIG. 3. Nonlinear Hall effect in $BaMnSb_2$. (a) E-ph renormalized Berry curvature dipole, $D_{yz}^{e\text{-ph}}$, as a function of Fermi level at four different temperatures. (b) Hall response $\chi_{xyy}/(\sigma_{xx}\sigma_{yy}^2)$ vs temperature, with response peaks normalized to 1 in all cases. Results are shown for three Fermi levels near the conduction band edge, which is taken as the energy zero in both panels.

previous calculations [36]. The nonmonotonic dependence on the Fermi level originates from two competing effects: an increasing number of thermally activated carriers due to increased density of states, and a decrease in the Berry curvature, as E_F increases away from the conduction band edge. At higher temperatures, the BCD decreases for a wide range of Fermi levels, and the 30-meV peak disappears progressively. We attribute these trends to the increasing strength of e-ph interactions at higher temperatures and to the thermal excitation of carriers near the Fermi level, both of which smooth out the 30-meV peak.

A quantity suitable for direct comparison with experiments is the Hall response V_{xyy}/I_y^2, where V_{xyy} is the nonlinear Hall voltage generated along the x direction when a current I_y is applied along the y axis. A simple calculation (see SM [60]) shows that the quantity V_{xyy}/I_y^2 measured in experiments is proportional to $\chi_{xyy}/\sigma_{xx}\sigma_{yy}^2$. We compute this quantity for $BaMnSb_2$ in Fig. 3(b) and show it as a function of temperature for three values of the Fermi level near the BCD peak. The Hall response for E_F=20 meV shows a peak around 200 K, which is qualitatively consistent with the experimental observation of a nonlinear Hall response peak at high temperature [36]. The position of this peak is sensitive to the Fermi level, and small changes in E_F substantially change the temperature trend. Note also that all responses depend on both second-order conductivities χ_{xyy} and linear conductivities (σ_{xx} and σ_{yy}). Therefore, calculations of NLHE based only on BCD cannot provide quantitative predictions of the nonlinear Hall response because the scattering time τ and its temperature dependence are also needed. This further highlights the importance of accurately modeling electron scattering to study the NLHE.

In conclusion, this work demonstrates a unified quantitative framework to study magnetotransport and the nonlinear Hall response in quantum materials, advancing their microscopic understanding. Our approach combines two pillars of modern first-principles calculations: electronic band structure and wave functions to describe the band topology, and e-ph interactions and the Boltzmann equation to model transport properties and temperature dependence. We have shown that this method can correctly predict the magnetoresistance in the semiclassical regime in a topological semimetal and resolve its Lorentz and chiral contributions. Our analysis of the NLHE in bulk and two-dimensional materials highlights the strong effects of the e-ph interactions on the Berry curvature dipole and nonlinear Hall response.

The method shown here adds to the first-principles toolkit for studying quantum materials and can be extended in multiple ways. Future work will expand the formalism to include electron-defect scattering at low temperature [71,72] as well as consider Berry curvature multipoles, magnetism, and quantum-metric effects [20].

D.C.D. thanks Yao Luo for fruitful discussions. This work was supported by the National Science Foundation under Grant No. OAC-2209262. L.A.T. is supported by the National Science Foundation Graduate Research Fellowship under Grant No. 2139433. J.-J.Z. is supported by the National Natural Science Foundation of China (Grant No. 12104039). J.P. is supported by the Glocal University 30 project (Grant No. 2.0081021.03). This research used resources of the National Energy Research Scientific Computing Center, a DOE Office of Science User Facility supported by the Office of Science of the U.S. Department of Energy under Contract No. DE-AC02-05CH11231 using NERSC award No. DDR-ERCAP0026831.

Data availability. The data that support the findings of this Letter are openly available [73].

[1] C. L. Kane and E. J. Mele, Quantum spin Hall effect in graphene, Phys. Rev. Lett. **95**, 226801 (2005).

[2] X.-L. Qi and S.-C. Zhang, Topological insulators and superconductors, Rev. Mod. Phys. **83**, 1057 (2011).

[3] M. Z. Hasan and C. L. Kane, *Colloquium*: Topological insulators, Rev. Mod. Phys. **82**, 3045 (2010).

[4] L. Fu and C. L. Kane, Superconducting proximity effect and Majorana fermions at the surface of a topological insulator, Phys. Rev. Lett. **100**, 096407 (2008).

[5] B. A. Bernevig, T. L. Hughes, and S.-C. Zhang, Quantum spin Hall effect and topological phase transition in HgTe quantum wells, Science **314**, 1757 (2006).

[6] X.-L. Qi and S.-C. Zhang, The quantum spin Hall effect and topological insulators, Phys. Today **63**(1), 33 (2010).

[7] Z. Zhang, N. Wang, N. Cao, A. Wang, X. Zhou, K. Watanabe, T. Taniguchi, B. Yan, and W.-B. Gao, Controlled large nonreciprocal charge transport in an intrinsic magnetic topological insulator MnBi2Te4, Nat. Commun. **13**, 6191 (2022).

[8] A. Farrell and T. Pereg-Barnea, Edge-state transport in Floquet topological insulators, Phys. Rev. B **93**, 045121 (2016).

[9] D. Hsieh, Y. Xia, D. Qian, L. Wray, J. H. Dil, F. Meier, J. Osterwalder, L. Patthey, J. G. Checkelsky, N. P. Ong, A. V. Fedorov, H. Lin, A. Bansil, D. Grauer, Y. S. Hor, R. J. Cava, and M. Z. Hasan, A tunable topological insulator in the spin helical Dirac transport regime, Nature (London) **460**, 1101 (2009).

[10] M. He, H. Sun, and Q. L. He, Topological insulator: Spintronics and quantum computations, Front. Phys. **14**, 43401 (2019).

[11] Q. L. He, T. L. Hughes, N. P. Armitage, Y. Tokura, and K. L. Wang, Topological spintronics and magnetoelectronics, Nat. Mater. **21**, 15 (2022).

[12] N. P. Armitage, E. J. Mele, and A. Vishwanath, Weyl and Dirac semimetals in three-dimensional solids, Rev. Mod. Phys. **90**, 015001 (2018).

[13] A. A. Zyuzin and A. A. Burkov, Topological response in Weyl semimetals and the chiral anomaly, Phys. Rev. B **86**, 115133 (2012).

[14] N. P. Ong and S. Liang, Experimental signatures of the chiral anomaly in Dirac–Weyl semimetals, Nat. Rev. Phys. **3**, 394 (2021).

[15] Z. Z. Du, H.-Z. Lu, and X. C. Xie, Nonlinear Hall effects, Nat. Rev. Phys. **3**, 744 (2021).

[16] I. Sodemann and L. Fu, Quantum nonlinear Hall effect induced by Berry curvature dipole in time-reversal invariant materials, Phys. Rev. Lett. **115**, 216806 (2015).

[17] M. Suárez-Rodríguez, F. De Juan, I. Souza, M. Gobbi, F. Casanova, and L. E. Hueso, Nonlinear transport in noncentrosymmetric systems, Nat. Mater. **24**, 1005 (2025).

[18] N. Wang, D. Kaplan, Z. Zhang, T. Holder, N. Cao, A. Wang, X. Zhou, F. Zhou, Z. Jiang, C. Zhang, *et al.*, Quantum-metric-induced nonlinear transport in a topological antiferromagnet, Nature (London) **621**, 487 (2023).

[19] C. Wang, Y. Gao, and D. Xiao, Intrinsic nonlinear Hall effect in antiferromagnetic tetragonal CuMnAs, Phys. Rev. Lett. **127**, 277201 (2021).

[20] Y. Fang, J. Cano, and S. A. A. Ghorashi, Quantum geometry induced nonlinear transport in altermagnets, Phys. Rev. Lett. **133**, 106701 (2024).

[21] H. B. Nielsen and M. Ninomiya, The Adler-Bell-Jackiw anomaly and Weyl fermions in a crystal, Phys. Lett. B **130**, 389 (1983).

[22] J. Xiong, S. K. Kushwaha, T. Liang, J. W. Krizan, M. Hirschberger, W. Wang, R. J. Cava, and N. P. Ong, Evidence for the chiral anomaly in the Dirac semimetal Na_3Bi, Science **350**, 413 (2015).

[23] X. Huang, L. Zhao, Y. Long, P. Wang, D. Chen, Z. Yang, H. Liang, M. Xue, H. Weng, Z. Fang, X. Dai, and G. Chen, Observation of the chiral-anomaly-induced negative magnetoresistance in 3D Weyl semimetal TaAs, Phys. Rev. X **5**, 031023 (2015).

[24] C.-Z. Li, L.-X. Wang, H. Liu, J. Wang, Z.-M. Liao, and D.-P. Yu, Giant negative magnetoresistance induced by the chiral anomaly in individual Cd_3As_2 nanowires, Nat. Commun. **6**, 10137 (2015).

[25] C.-L. Zhang, S.-Y. Xu, I. Belopolski, Z. Yuan, Z. Lin, B. Tong, G. Bian, N. Alidoust, C.-C. Lee, S.-M. Huang, *et al.*, Signatures of the Adler–Bell–Jackiw chiral anomaly in a Weyl fermion semimetal, Nat. Commun. **7**, 10735 (2016).

[26] S. Liang, J. Lin, S. Kushwaha, J. Xing, N. Ni, R. J. Cava, and N. P. Ong, Experimental tests of the chiral anomaly magnetoresistance in the Dirac-Weyl semimetals Na_3Bi and GdPtBi, Phys. Rev. X **8**, 031002 (2018).

[27] M. Hirschberger, S. Kushwaha, Z. Wang, Q. Gibson, S. Liang, C. A. Belvin, B. A. Bernevig, R. J. Cava, and N. P. Ong, The chiral anomaly and thermopower of Weyl fermions in the half-Heusler GdPtBi, Nat. Mater. **15**, 1161 (2016).

[28] R. D. dos Reis, M. O. Ajeesh, N. Kumar, F. Arnold, C. Shekhar, M. Naumann, M. Schmidt, M. Nicklas, and E. Hassinger, On the search for the chiral anomaly in Weyl semimetals: The negative longitudinal magnetoresistance, New J. Phys. **18**, 085006 (2016).

[29] Y. Li, Z. Wang, P. Li, X. Yang, Z. Shen, F. Sheng, X. Li, Y. Lu, Y. Zheng, and Z.-A. Xu, Negative magnetoresistance in Weyl semimetals NbAs and NbP: Intrinsic chiral anomaly and extrinsic effects, Front. Phys. **12**, 127205 (2017).

[30] In this work, the term "topological materials" is used in a broad sense to describe systems possessing nonzero Berry curvature, giving rise to phenomena such as the chiral anomaly and the nonlinear Hall effect.

[31] Q. Ma, S.-Y. Xu, H. Shen, D. MacNeill, V. Fatemi, T.-R. Chang, A. M. Mier Valdivia, S. Wu, Z. Du, C.-H. Hsu, *et al.*, Observation of the nonlinear Hall effect under time-reversal-symmetric conditions, Nature (London) **565**, 337 (2019).

[32] M. Huang, Z. Wu, J. Hu, X. Cai, E. Li, L. An, X. Feng, Z. Ye, N. Lin, K. T. Law, and N. Wang, Giant nonlinear Hall effect in twisted bilayer WSe_2, Natl. Sci. Rev. **10**, nwac232 (2023).

[33] S.-C. Ho, C.-H. Chang, Y.-C. Hsieh, S.-T. Lo, B. Huang, T.-H.-Y. Vu, C. Ortix, and T.-M. Chen, Hall effects in artificially corrugated bilayer graphene without breaking time-reversal symmetry, Nat. Electron. **4**, 116 (2021).

[34] P. He, H. Isobe, D. Zhu, C.-H. Hsu, L. Fu, and H. Yang, Quantum frequency doubling in the topological insulator Bi_2Se_3, Nat. Commun. **12**, 698 (2021).

[35] A. Tiwari, F. Chen, S. Zhong, E. Drueke, J. Koo, A. Kaczmarek, C. Xiao, J. Gao, X. Luo, Q. Niu, Y. Sun, B. Yan, L. Zhao, and A. W. Tsen, Giant *c*-axis nonlinear anomalous Hall effect in Td-$MoTe_2$ and WTe_2, Nat. Commun. **12**, 2049 (2021).

[36] L. Min, H. Tan, Z. Xie, L. Miao, R. Zhang, S. H. Lee, V. Gopalan, C.-X. Liu, N. Alem, B. Yan, and Z. Mao, Strong room-temperature bulk nonlinear Hall effect in a spin-valley locked Dirac material, Nat. Commun. **14**, 364 (2023).

[37] K. Kang, T. Li, E. Sohn, J. Shan, and K. F. Mak, Nonlinear anomalous Hall effect in few-layer WTe_2, Nat. Mater. **18**, 324 (2019).

[38] O. O. Shvetsov, V. D. Esin, A. V. Timonina, N. N. Kolesnikov, and E. V. Deviatov, Nonlinear Hall effect in three-dimensional Weyl and Dirac semimetals, JETP Lett. **109**, 715 (2019).

[39] M.-S. Qin, P.-F. Zhu, X.-G. Ye, W.-Z. Xu, Z.-H. Song, J. Liang, K. Liu, and Z.-M. Lia, Strain tunable Berry curvature dipole, orbital magnetization and nonlinear Hall effect in WSe_2 monolayer, Chin. Phys. Lett. **38**, 017301 (2021).

[40] D. T. Son and B. Z. Spivak, Chiral anomaly and classical negative magnetoresistance of Weyl metals, Phys. Rev. B **88**, 104412 (2013).

[41] K.-S. Kim, H.-J. Kim, and M. Sasaki, Boltzmann equation approach to anomalous transport in a Weyl metal, Phys. Rev. B **89**, 195137 (2014).

[42] R. M. Martin, *Electronic Structure: Basic Theory and Practical Methods* (Cambridge University Press, Cambridge, 2004).

[43] N. Marzari, A. A. Mostofi, J. R. Yates, I. Souza, and D. Vanderbilt, Maximally localized Wannier functions: Theory and applications, Rev. Mod. Phys. **84**, 1419 (2012).

[44] X. Wang, J. R. Yates, I. Souza, and D. Vanderbilt, *Ab initio* calculation of the anomalous Hall conductivity by Wannier interpolation, Phys. Rev. B **74**, 195118 (2006).

[45] W. Feng, C.-C. Liu, G.-B. Liu, J.-J. Zhou, and Y. Yao, First-principles investigations on the Berry phase effect in spin–orbit coupling materials, Comput. Mater. Sci. **112**, 428 (2016).

[46] W. Li, Electrical transport limited by electron-phonon coupling from Boltzmann transport equation: An *ab initio* study of Si, Al, and MoS_2, Phys. Rev. B **92**, 075405 (2015).

[47] J.-J. Zhou and M. Bernardi, *Ab initio* electron mobility and polar phonon scattering in GaAs, Phys. Rev. B **94**, 201201(R) (2016).

[48] T. Sohier, D. Campi, N. Marzari, and M. Gibertini, Mobility of two-dimensional materials from first principles in an accurate and automated framework, Phys. Rev. Mater. **2**, 114010 (2018).

[49] N.-E. Lee, J.-J. Zhou, L. A. Agapito, and M. Bernardi, Charge transport in organic molecular semiconductors from first principles: The bandlike hole mobility in a naphthalene crystal, Phys. Rev. B **97**, 115203 (2018).

[50] F. Macheda and N. Bonini, Magnetotransport phenomena in *p*-doped diamond from first principles, Phys. Rev. B **98**, 201201(R) (2018).

[51] V. A. Jhalani, J.-J. Zhou, J. Park, C. E. Dreyer, and M. Bernardi, Piezoelectric electron-phonon interaction from *ab initio* dynamical quadrupoles: Impact on charge transport in wurtzite GaN, Phys. Rev. Lett. **125**, 136602 (2020).

[52] D. C. Desai, B. Zviazhynski, J.-J. Zhou, and M. Bernardi, Magnetotransport in semiconductors and two-dimensional materials from first principles, Phys. Rev. B **103**, L161103 (2021).

[53] D. J. Abramovitch, J.-J. Zhou, J. Mravlje, A. Georges, and M. Bernardi, Combining electron-phonon and dynamical mean-field theory calculations of correlated materials: Transport in the correlated metal Sr_2RuO_4, Phys. Rev. Mater. **7**, 093801 (2023).

[54] D. C. Desai, J. Park, J.-J. Zhou, and M. Bernardi, Dominant two-dimensional electron-phonon interactions in the bulk Dirac semimetal Na_3Bi, Nano Lett. **23**, 3947 (2023).

[55] Z. Liu, S. B. Mishra, J.-M. Lihm, S. Poncé, and E. R. Margine, Phonon-limited carrier transport in the Weyl semimetal TaAs, Phys. Rev. B **112**, 104311 (2025).

[56] J.-M. Lihm and C.-H. Park, Nonlinear Hall effect from long-lived valley-polarizing relaxons, Phys. Rev. Lett. **132**, 106402 (2024).

[57] G. Sundaram and Q. Niu, Wave-packet dynamics in slowly perturbed crystals: Gradient corrections and Berry-phase effects, Phys. Rev. B **59**, 14915 (1999).

[58] D. Xiao, M.-C. Chang, and Q. Niu, Berry phase effects on electronic properties, Rev. Mod. Phys. **82**, 1959 (2010).

[59] M. P. Marder, *Condensed Matter Physics* (Wiley, New York, 2010), p. 428.

[60] See Supplemental Material at http://link.aps.org/supplemental/10.1103/fl5l-dhn3 for additional derivations, computational details, adaptive **k**-point sampling near the Weyl nodes, and discussion of the breakdown of the semiclassical limit, which includes Refs. [74–77].

[61] For topologically trivial materials the Berry curvature $\mathbf{\Omega}_{n\mathbf{k}}$ vanishes, and Eq. (2) becomes identical to the BTE with both electric and magnetic fields derived previously in Ref. [52].

[62] J.-J. Zhou, J. Park, I.-T. Lu, I. Maliyov, X. Tong, and M. Bernardi, Perturbo: A software package for *ab initio* electron–phonon interactions, charge transport and ultrafast dynamics, Comput. Phys. Commun. **264**, 107970 (2021).

[63] D. Xiao, J. Shi, and Q. Niu, Berry phase correction to electron density of states in solids, Phys. Rev. Lett. **95**, 137204 (2005).

[64] P. Giannozzi, S. Baroni, N. Bonini, M. Calandra, R. Car, C. Cavazzoni, D. Ceresoli, G. L. Chiarotti, M. Cococcioni, I. Dabo, *et al.*, QUANTUM ESPRESSO: A modular and open-source software project for quantum simulations of materials, J. Phys.: Condens. Matter **21**, 395502 (2009).

[65] P. Giannozzi, Jr., O. Andreussi, T. Brumme, O. Bunau, M. B. Nardelli, M. Calandra, R. Car, C. Cavazzoni, D. Ceresoli, M. Cococcioni, *et al.*, Advanced capabilities for materials modelling with QUANTUM ESPRESSO, J. Phys.: Condens. Matter **29**, 465901 (2017).

[66] G. Pizzi, V. Vitale, R. Arita, S. Blügel, F. Freimuth, G. Géranton, M. Gibertini, D. Gresch, C. Johnson, T. Koretsune, *et al.*, Wannier90 as a community code: New features and applications, J. Phys.: Condens. Matter **32**, 165902 (2020).

[67] G. E. Allemand, M. Giantomassi, and M. J. Verstraete, First-principles calculations of transport coefficients in the Weyl semimetal TaAs, Phys. Rev. B **112**, 125122 (2025).

[68] J. Buckeridge, D. Jevdokimovs, C. R. A. Catlow, and A. A. Sokol, Bulk electronic, elastic, structural, and dielectric properties of the Weyl semimetal TaAs, Phys. Rev. B **93**, 125205 (2016).

[69] L. X. Yang, Z. K. Liu, Y. Sun, H. Peng, H. F. Yang, T. Zhang, B. Zhou, Y. Zhang, Y. F. Guo, M. Rahn, D. Prabhakaran, Z. Hussain, S.-K. Mo, C. Felser, B. Yan, and Y. L. Chen, Weyl semimetal phase in the non-centrosymmetric compound TaAs, Nat. Phys. **11**, 728 (2015).

[70] J.-S. You, S. Fang, S.-Y. Xu, E. Kaxiras, and T. Low, Berry curvature dipole current in the transition metal dichalcogenides family, Phys. Rev. B **98**, 121109(R) (2018).

[71] I.-T. Lu, J.-J. Zhou, and M. Bernardi, Efficient *ab initio* calculations of electron-defect scattering and defect-limited carrier mobility, Phys. Rev. Mater. **3**, 033804 (2019).

[72] I.-T. Lu, J.-J. Zhou, J. Park, and M. Bernardi, First-principles ionized-impurity scattering and charge transport in doped materials, Phys. Rev. Mater. **6**, L010801 (2022).

[73] D. C. Desai, L. A. Tan, J.-J. Zhou, S. Peng, J. Park, and M. Bernardi, Magnetotransport in topological materials and

nonlinear Hall effect via first-principles electronic interactions and band topology, Materials Cloud Archive, 2026.55 (2026), https://doi.org/10.24435/materialscloud:a7-ff.

[74] J. Heyd, G. E. Scuseria, and M. Ernzerhof, Hybrid functionals based on a screened Coulomb potential, J. Chem. Phys. **118**, 8207 (2003).

[75] J. P. Perdew, A. Ruzsinszky, G. I. Csonka, O. A. Vydrov, G. E. Scuseria, L. A. Constantin, X. Zhou, and K. Burke, Restoring the density-gradient expansion for exchange in solids and surfaces, Phys. Rev. Lett. **100**, 136406 (2008).

[76] S. Huang, J. Kim, W. A. Shelton, E. W. Plummer, and R. Jin, Nontrivial Berry phase in magnetic $BaMnSb_2$ semimetal, Proc. Natl. Acad. Sci. USA **114**, 6256 (2017).

[77] S. S. Tsirkin, High performance Wannier interpolation of Berry curvature and related quantities with WannierBerri code, npj Comput. Mater. **7**, 33 (2021).